Energy Absorption in Glass-Reinforced Continuous Strand Mat Composites

George C. Jacob,[1] J. Michael Starbuck,[2] Srdan Simunovic,[3] John F. Fellers[1]

[1]*Materials Science and Engineering Department, University of Tennessee, Knoxville, 434 Dougherty Engineering, Knoxville, Tennessee 37996*
[2]*Polymer Matrix Composites Group, Metals and Ceramics Division, Oak Ridge National Laboratory, Post Office Box 2009, Oak Ridge, Tennessee 37831-8048*
[3]*Computational Material Science, Computer Science and Mathematics Division, Oak Ridge National Laboratory, Post Office Box 2008, Bldg. 6025, MS-6359, Oak Ridge, Tennessee 37831-6359*

Received 28 December 2002; accepted 2 April 2003

ABSTRACT: A unique test fixture was developed for determining the energy-absorbing mechanisms in automotive composite material systems. The objective of the test method was to quantify the energy absorption and identify the failure mechanisms associated with the observed frond formation in progressive crush testing of composite tubes by testing less costly composite plates under progressive crush load conditions. Quasi-static progressive crush tests were performed on glass/polyurethane continuous strand mat (CSM) composite plate specimens. The effect of various test parameters on energy absorption was evaluated by varying the following parameters during testing: the loading rate, profile radius, and profile constraint condition. The experimental data in conjunction with the test observations were used to develop analytical models for predicting the crashworthiness of automotive composite structures. The crushing process and the load-deflection curves were similar to the progressive crushing of tubes. Modification of the basic specimen geometry was required when testing material systems that have low axial stiffness to prevent a global buckling mode. © 2003 Wiley Periodicals, Inc. J Appl Polym Sci 90: 3222–3232, 2003

Key words: polyurethanes; glass; composite; polymer; crashworthiness

INTRODUCTION

In passenger vehicles, the ability to absorb impact energy and be survivable for the occupant is called the "crash worthiness" of the structure. This absorption of energy is through controlled failure mechanisms and modes that enable the maintenance of a gradual decay in the load profile.

Current legislation for automobiles requires that vehicles be designed such that, in the event of an impact at speeds up to 15.5 m/s (35 mph) with a solid, immovable object, the occupants of the passenger compartment should not experience a resulting force that produces a net deceleration greater than 20 g.[1] Crashworthy structures should be designed to absorb impact energy in a controlled manner, thereby bringing the passenger compartment to rest without the occupant being subjected to high deceleration, which can cause serious internal injury, particularly brain damage.

In the crashworthiness of automotive structures, the primary issues to the automotive industry are the overall economy and the weight of the material. To reduce the weight and improve the fuel economy, polymer composite materials have replaced more and more metal parts in vehicles. The tailorability of composites, in addition to their attributes of high strength-to-weight and stiffness-to-weight ratios, corrosion resistance, and fatigue resistance, makes them very attractive for designing crashworthy structures. The challenge is determining what specific design features are needed in the geometry and what material systems will enable greater safety without negatively affecting the overall economics of fabrication and production.

The crashworthiness of a material is expressed in terms of its specific energy absorption (SEA), which is characteristic to that particular material. It is defined as the energy absorbed per unit mass of crushed material. Mathematically, SEA $= W/(V\rho)$, where the total energy absorbed, W, is calculated by integrating the area under the load-deflection curve, V is the volume of crushed material, and ρ is the density of the material.

In comparison to metals, most composites are generally characterized by a brittle rather than a ductile response to the applied loads, especially in compression. The major difference, however, is that metal structures collapse under crush or impact by buckling and/or folding in accordion-type fashion involving extensive plastic deformation, whereas composites fail through a sequence of fracture mechanisms. The actual mechanisms, for example, fiber fracture, matrix

Correspondence to: G. C. Jacob (mailto:gjacob@utk.edu).

Journal of Applied Polymer Science, Vol. 90, 3222–3232 (2003)

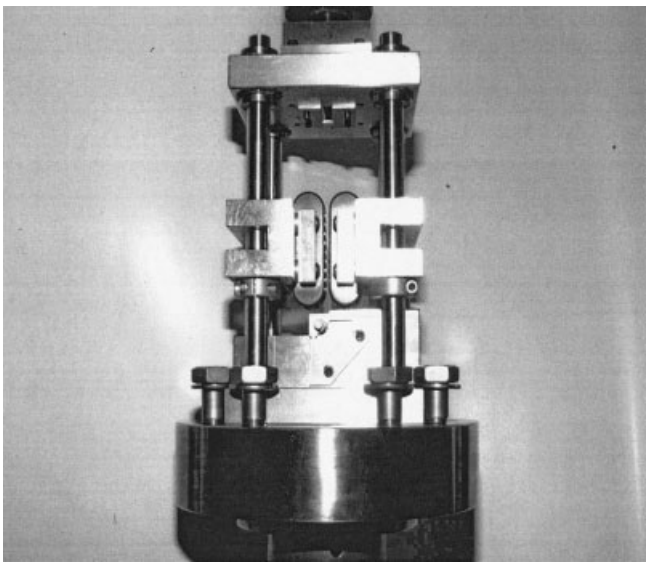

Figure 1 Text fixture assembly.

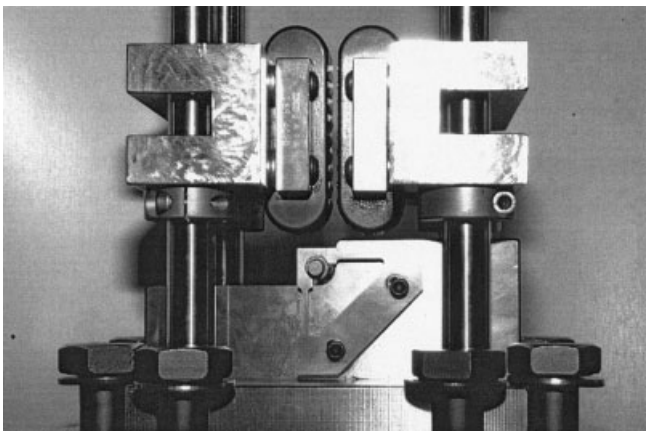

Figure 2 Roller ways and contact profile constraint.

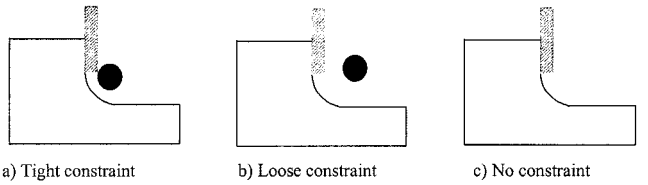

Figure 3 Constraint conditions.

crazing and cracking, fiber–matrix debonding, delamination, and interply separation, and sequence of damage are highly dependent on lamina orientation, crush speed, triggers, and geometry of the structure.

Much of the experimental work to study the effects of fiber type, matrix type, fiber architecture, specimen geometry, and loading rate on the energy absorption of composite materials has been carried out on axisymmetric tubes.[2–29] Tube structures are relatively easy to fabricate and close to the geometry of the actual crashworthy structures. In the progressive crushing of composite tubes, there are many different failure mechanisms that contribute to the overall energy absorption of the structure. To isolate the damage mechanisms and quantify the energy absorbed by glass-reinforced continuous strand mat composites, plate specimens of glass/polyurethane were tested using a unique test fixture.

EXPERIMENTAL

Material system investigated: glass-reinforced continuous strand mat (CSM)

The CSM specimens were machined from plates that were fabricated using glass-fiber reinforcement in a

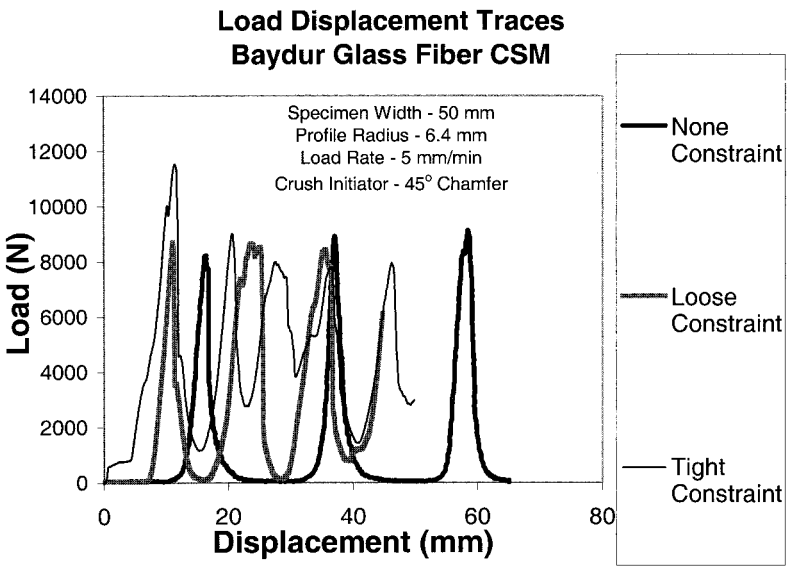

Figure 4 Load-displacement traces for CSM.

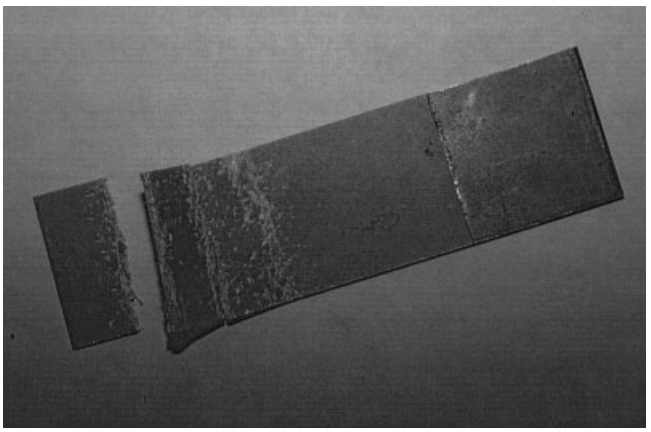

Figure 5 Crushed CSM specimen.

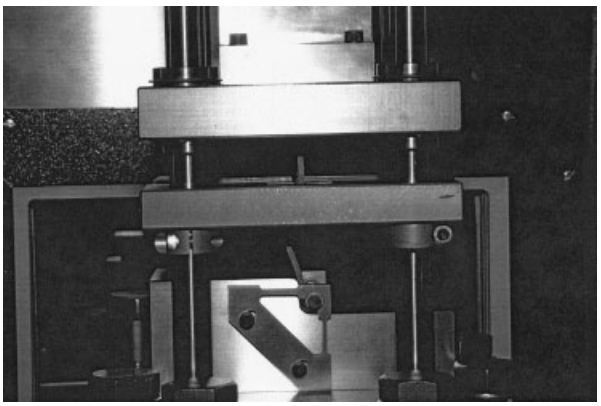

Figure 6 Specimen buckling during crushing of CSM in loose-constraint condition.

TABLE I
Experimental Data from Tests Conducted with a Profile Block of Radius 0.635 cm at 0.5 cm/min Loading Rate on CSM

Specimen no.	Specimen width (cm)	Profile radius (cm)	Constraint	Load rate (cm/min)	Initial peak load (N)	Maximum peak load (N)	Sustained crush load (N)	SEA (J/g)	Average SEA (J/g)
CSM-1	5.070	0.635	None	0.5	7478.2	9556.5	4829.1	10.79	
CSM-2	5.071	0.635	None	0.5	7867.3	9487.0	4657.5	10.25	
CSM-3	5.073	0.635	None	0.5	8157.8	9064.7	4443.9	9.71	
CSM-4	5.070	0.635	None	0.5	8334.2	9460.9	4560.6	10.10	
CSM-5	5.072	0.635	None	0.5	7986.5	9123.5	4615.4	10.15	10.20
CSM-6	5.074	0.635	Loose	0.5	10611.2	10611.2	4600.6	21.79	
CSM-7	5.078	0.635	Loose	0.5	9209.2	9209.2	4081.3	16.96	
CSM-8	5.116	0.635	Loose	0.5	11852.5	11852.5	4652.1	21.80	
CSM-9	5.100	0.635	Loose	0.5	10932.8	10932.8	3950.1	16.39	
CSM-10	5.157	0.635	Loose	0.5	8679.9	8679.9	4238.7	19.95	19.38
CSM-11	5.096	0.635	Tight	0.5	9922.8	11412.3	5892.7	26.39	
CSM-12	5.086	0.635	Tight	0.5	6774.8	8688.3	5838.4	29.37	
CSM-13	5.106	0.635	Tight	0.5	7568.4	7568.4	4193.9	23.74	
CSM-14	5.097	0.635	Tight	0.5	7786.8	8675.4	5676.8	27.82	
CSM-15	5.100	0.635	Tight	0.5	8876.4	8876.4	5234.4	25.18	26.50

TABLE II
Experimental Data from Tests Conducted with a Profile Block of Radius 0.635 cm at 5 cm/min Loading Rate on CSM

Specimen no.	Specimen width (cm)	Profile radius (cm)	Constraint	Load rate (cm/min)	Initial peak load (N)	Maximum peak load (N)	Sustained crush load (N)	SEA (J/g)	Average SEA (J/g)
CSM-16	5.114	0.635	None	5	8313.2	10046.9	4542.5	11.10	
CSM-17	5.110	0.635	None	5	8319.3	8749.3	4413.3	10.79	
CSM-18	5.110	0.635	None	5	8234.7	9008.7	4540.0	11.05	
CSM-19	5.112	0.635	None	5	8303.6	8965.5	4512.7	11.00	
CSM-20	5.112	0.635	None	5	8298.6	8800.8	4419.0	10.80	10.95
CSM-21	5.098	0.635	Loose	5	8968.4	8968.4	4700.9	16.54	
CSM-22	5.111	0.635	Loose	5	9827.1	9827.1	3929.7	16.36	
CSM-23	5.111	0.635	Loose	5	9600.9	9600.9	3931.0	16.38	
CSM-24	5.110	0.635	Loose	5	9008.7	9008.7	4700.8	16.53	
CSM-25	5.098	0.635	Loose	5	9465.0	9465.0	4567.6	16.44	16.45
CSM-26	5.103	0.635	Tight	5	8575.7	9143.4	5720.8	22.67	
CSM-27	5.114	0.635	Tight	5	8767.6	9200.9	5734.7	22.72	
CSM-28	5.104	0.635	Tight	5	8500.9	9345.6	5674.5	22.50	
CSM-29	5.110	0.635	Tight	5	8798.9	9243.8	5730.0	22.71	
CSM-30	5.103	0.635	Tight	5	8567.9	9100.5	5735.4	22.80	22.68

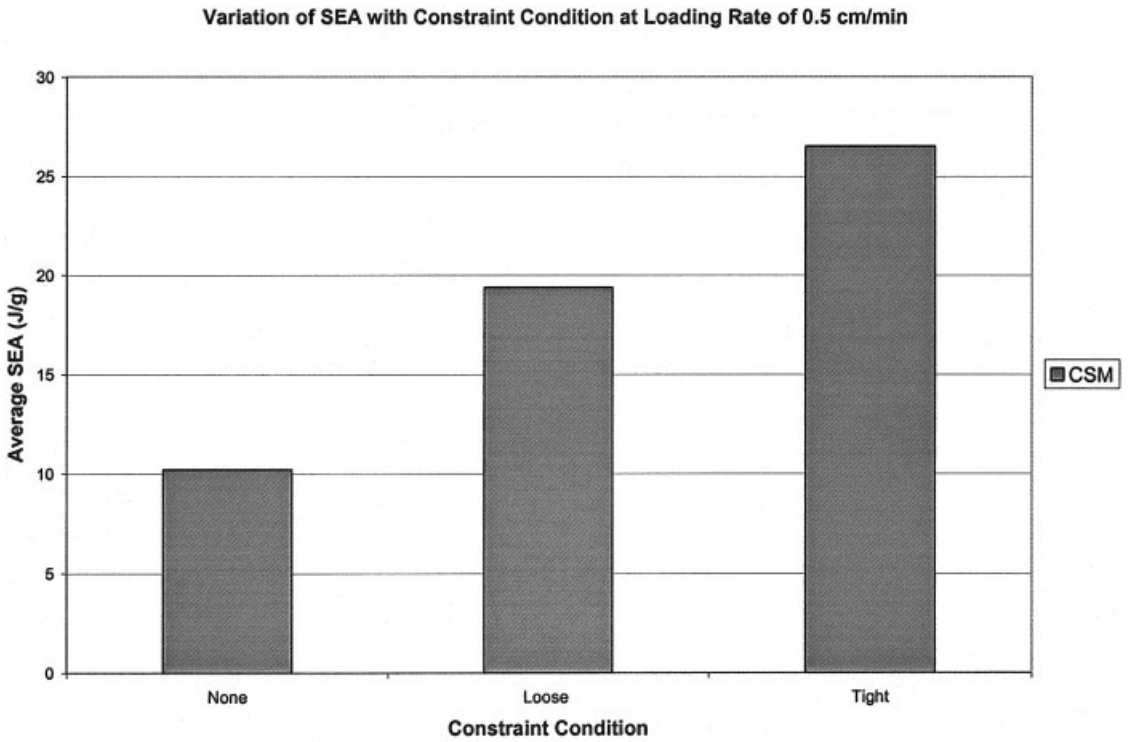

Figure 7 Variation of SEA with constraint condition at loading rate of 0.5 cm/min for CSM.

Baydur polyurethane resin. Glass fibers are cheap to buy and this makes them cost effective for automotive applications. Use of polyurethane as the resin is favored from its cost standpoint, as there are a large number of low-temperature processing techniques for polyurethane resins available to the industry that

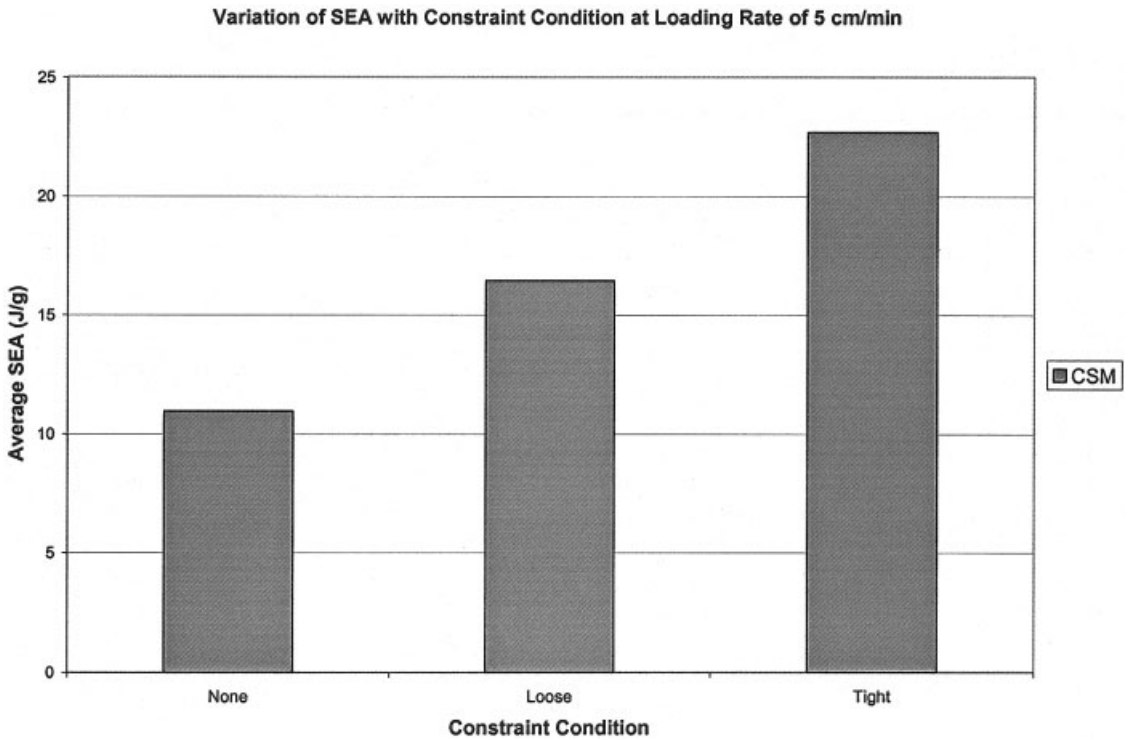

Figure 8 Variation of SEA with constraint condition at loading rate of 5 cm/min for CSM.

TABLE III
Experimental Data from Tests Conducted in the No-constraint Condition on CSM

Specimen no.	Specimen width (cm)	Profile radius (cm)	Constraint	Load rate (cm/min)	Initial peak load (N)	Maximum peak load (N)	Sustained crush load (N)	SEA (J/g)	Average SEA (J/g)
CSM-1	5.070	0.635	None	0.5	7478.2	9556.5	4829.1	10.79	
CSM-2	5.071	0.635	None	0.5	7867.3	9487.0	4657.5	10.25	
CSM-3	5.073	0.635	None	0.5	8157.8	9064.7	4443.9	9.71	
CSM-4	5.070	0.635	None	0.5	8334.2	9460.9	4560.6	10.10	
CSM-5	5.072	0.635	None	0.5	7986.5	9123.5	4615.4	10.15	10.20
CSM-16	5.114	0.635	None	5	8313.2	10046.9	4542.5	11.10	
CSM-17	5.110	0.635	None	5	8319.3	8749.3	4413.3	10.79	
CSM-18	5.110	0.635	None	5	8234.7	9008.7	4540.0	11.05	
CSM-19	5.112	0.635	None	5	8303.6	8965.5	4512.7	11.00	
CSM-20	5.112	0.635	None	5	8298.6	8800.8	4419.0	10.80	10.95

make it very cost efficient to manufacture them. Polyurethane resins, due to their low viscosity, wet the fiber better, thus strengthening the interfacial bonding between the matrix and reinforcement. Good interfacial bonding prevents the formation of instabilities around the fibers that cause the formation of microcracks and initiate failure. For polyurethane resins, adjusting their molecular structure can vary the glass transition temperature, T_g. The energy-absorption capability of a test specimen would be greatest if its glass transition temperature is near the test temperature. This is because the viscous response time of the specimen is in tune to the rate of energy absorption near its glass transition temperature. We can, therefore, spread the T_g over a wide range of temperatures by combining polyurethanes of different molecular structures. Hence, we can expect to have high-energy absorption capabilities for the composite.

Test method

A new test fixture design was developed for determining the deformation behavior and damage mechanisms that occur during progressive crushing of composite materials. Composite plate specimens are very cheap to fabricate and it has been observed that plate specimens progressively crush in modes very similar to the damage modes that occur during the progressive crushing of composite tubes. Practical considerations related to the cost production of the test specimens were of paramount importance in developing the test methodology to be used in the fixture. Also, plates can be easily produced with consistently high quality. The fixture was designed to isolate the damage modes associated with the frond formation (splaying mode) in composite tubes by testing plate geometries.

The design is a modified version of an existing test fixture used for crush testing of composite plates.[30] Features incorporated into the design include an observable crush zone, long crush length, interchangeable contact profile, frictionless roller for contact constraint, and out-of-plane roller supports to prevent buckling (see Figs. 1–3). The brackets on either side of the profile plate were designed to provide a method of constraining the specimen to deform along the path of the contact profile. Using oil-impregnated bronze sleeve bearings in each bracket and installing a precision ground shaft that acts as a roller accomplish this. The severity of the contact profile constraint is determined by the position of the load cell brackets and is adjustable using slotted positioning holes. More details of the fixture design were provided by Starbuck et al.[31]

Testing procedure

The specimens had a nominal length of 178 mm and a width of 50 mm and a 45° chamfer was used as the

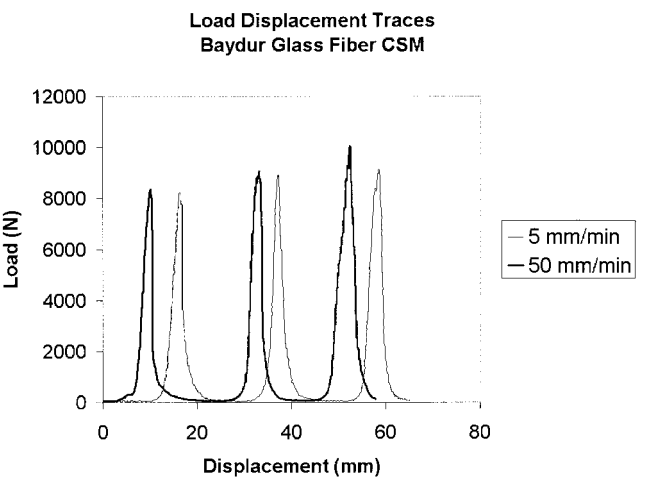

Figure 9 Load-displacement traces for a test conducted on CSM in the no-constraint condition at loading rates of 0.5 and 5 cm/min.

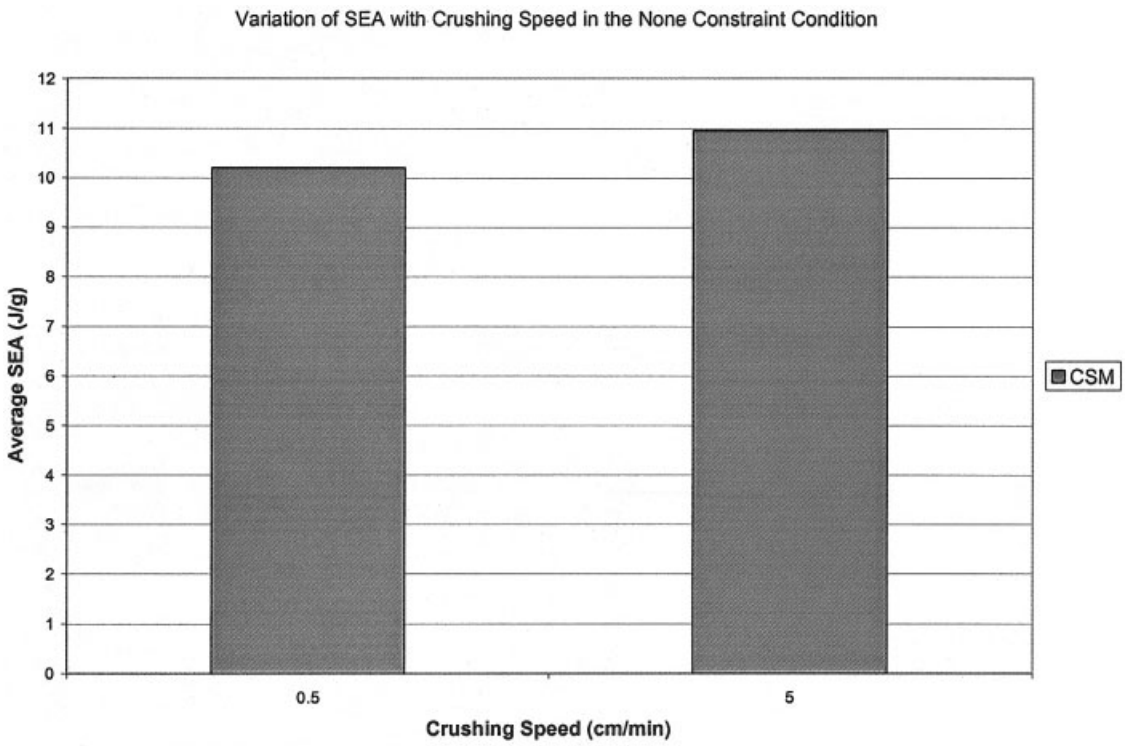

Figure 10 Variation of SEA with crushing speed for CAM in the no-constraint condition.

crush initiator. A diamond cutoff wheel was used to cut the specimens off the composite panel. No coolant was used during cutting, to prevent contamination of the test specimens. A loading rate of 5.0 and 50 mm/min and a profile block of radius 6.4 and 13 mm were used throughout the entire testing.

The MTS machine (Model 810, axial/torsional mode) used for testing had a load capacity of 50,000 lbs. An MTS Model 407 controller, which is a single-channel, digitally supervised proportional, integral, derivative, feed-forward (PIDF) servocontroller, was used to provide complete control of one servohydraulic channel/station in the MTS testing system. The load-deflection response was recorded using a computerized data-acquisition system. A 16-bit, 100-kHz National instrument data-acquisition card numbered pci6031E was used.

The SEA of a composite material, defined as the energy absorbed per unit mass of the material, is equal to W/m, where W is the total energy absorbed in the crushing of the composite plate specimen, which is the area under the load-displacement curve. From SEA $= W/m$, one can write SEA $= W/V\rho$, where V is the volume of the crushed portion of the composite plate specimen, and ρ, the density of the composite material. One can also write SEA $= W/(AL\rho)$, where A and

TABLE IV
Experimental Data from Tests Conducted in the Loose-constraint Condition on CSM

Specimen no.	Specimen width (cm)	Profile radius (cm)	Constraint	Load rate (cm/min)	Initial peak load (N)	Maximum peak load (N)	Sustained crush load (N)	SEA (J/g)	Average SEA (J/g)
CSM-6	5.074	0.635	Loose	0.5	10611.2	10611.2	4600.6	21.79	
CSM-7	5.078	0.635	Loose	0.5	9209.2	9209.2	4081.3	16.96	
CSM-8	5.116	0.635	Loose	0.5	11852.5	11852.5	4652.1	21.80	
CSM-9	5.100	0.635	Loose	0.5	10932.8	10932.8	3950.1	16.39	
CSM-10	5.157	0.635	Loose	0.5	8679.9	8679.9	4238.7	19.95	19.38
CSM-21	5.098	0.635	Loose	5	8968.4	8968.4	4700.9	16.54	
CSM-22	5.111	0.635	Loose	5	9827.1	9827.1	3929.7	16.36	
CSM-23	5.111	0.635	Loose	5	9600.9	9600.9	3931.0	16.38	
CSM-24	5.110	0.635	Loose	5	9008.7	9008.7	4700.8	16.53	
CSM-25	5.098	0.635	Loose	5	9465.0	9465.0	4567.6	16.44	16.45

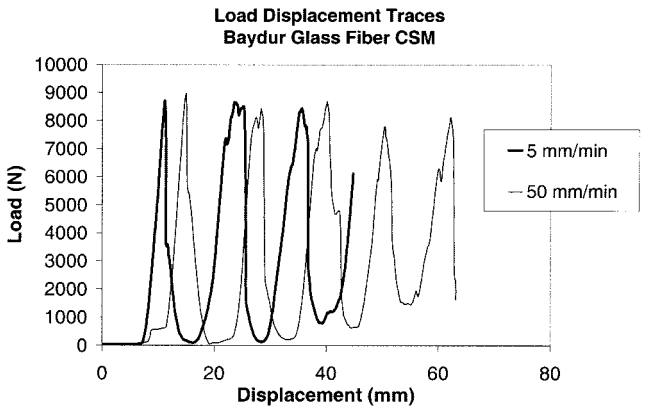

Figure 11 Load-displacement traces for a test conducted on CSM in the loose-constraint condition at loading rates of 0.5 and 5 cm/min.

L are the cross-sectional area and length of the crushed portion of the composite plate specimen, respectively. SEA = $W/(AL\rho)$ was used to calculate the SEA of all the composite plate specimens tested.

Variables investigated

The effects of the loading rate, profile constraint, and profile shape on the energy-absorbing characteristics of the CSM composites were studied. Below is a summary of the various test variables that were investigated:

- Profile radius: 6.4 mm (0.25 in.) and 13 mm (0.5 in.).
- Constraint: none, loose, tight.
- Loading rate: 5 mm/min (0.2 in./min) and 50 mm/min (2 in./min).

RESULTS AND DISCUSSION

In the CSM specimens, finite-length fractures across the entire width were observed. For a comparison of the load-displacement traces recorded for a test conducted on a specimen in the no-constraint, the loose-constraint, and the tight-constraint conditions, see Figure 4.

For tests conducted in the no- and loose-constraint conditions, the load would monotonically increase until fracture occurred and then the load would decrease to almost zero (see Fig. 4). Approximately the same magnitude of load was measured at each of the fracture points and fracture lengths were approximately the same (see Fig. 5).

Effect of constraint

The tests conducted on the CSM material were only successful when the roller was positioned in the no-constraint condition. When the loose- or tight-constraint condition was attempted, the initial peak load increased and the CSM specimens buckled between the top plate and roller ways. Figure 6 shows speci-

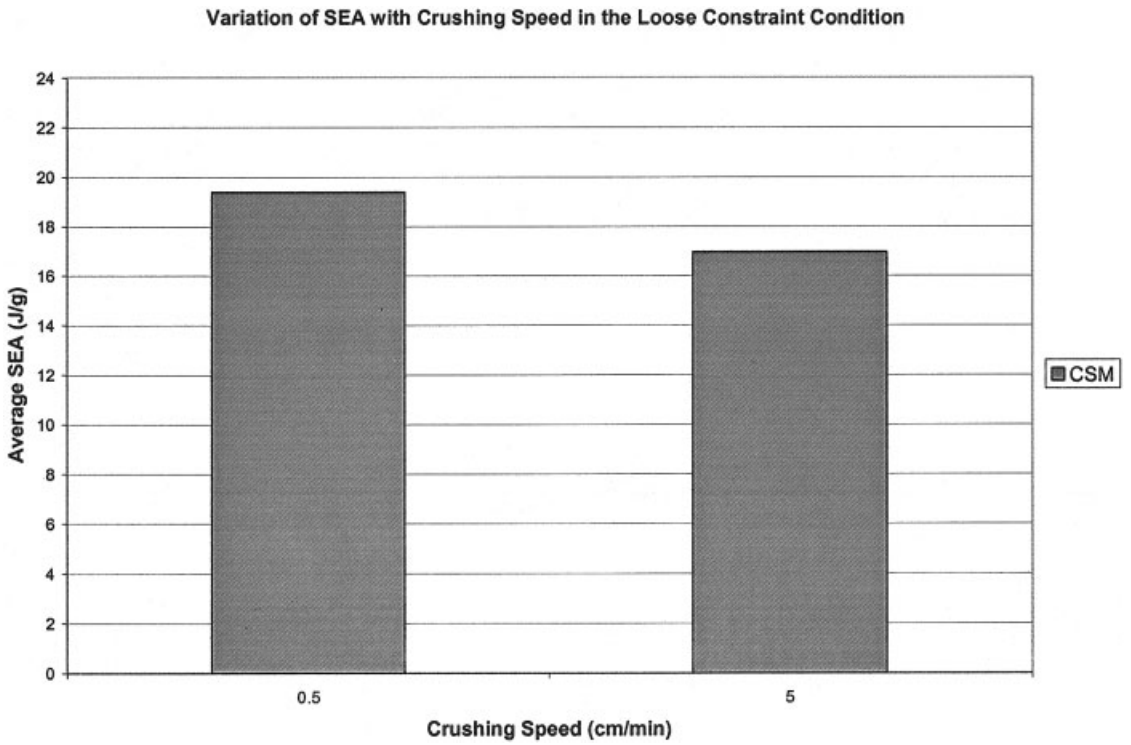

Figure 12 Variation of SEA with crushing speed for CSM in the loose-constraint condition.

TABLE V
Experimental Data from Tests Conducted in the Tight-constraint Condition on CSM

Specimen no.	Specimen width (cm)	Profile radius (cm)	Constraint	Load rate (cm/min)	Initial peak load (N)	Maximum peak load (N)	Sustained crush load (N)	SEA (J/g)	Average SEA (J/g)
CSM-11	5.096	0.635	Tight	0.5	9922.8	11412.3	5892.7	26.39	
CSM-12	5.086	0.635	Tight	0.5	6774.8	8688.3	5838.4	29.37	
CSM-13	5.106	0.635	Tight	0.5	7568.4	7568.4	4193.9	23.74	
CSM-14	5.097	0.635	Tight	0.5	7786.8	8675.4	5676.8	27.82	
CSM-15	5.100	0.635	Tight	0.5	8876.4	8876.4	5234.4	25.18	26.50
CSM-26	5.103	0.635	Tight	5	8575.7	9143.4	5720.8	22.68	
CSM-27	5.114	0.635	Tight	5	8767.6	9200.9	5734.7	22.72	
CSM-28	5.104	0.635	Tight	5	8500.9	9345.6	5674.5	22.50	
CSM-29	5.110	0.635	Tight	5	8798.9	9243.8	5730.0	22.71	
CSM-30	5.103	0.635	Tight	5	8567.9	9100.5	5735.4	22.80	22.68

men buckling when a test was conducted on the CSM material in the loose-constraint condition. The roller ways were unsuccessful in preventing out-of-plane buckling in the CSM material because of its low buckling strength. This resulted in having to use a metal push plate to reduce the unsupported specimen length. The metal plate was 76 mm in length and was bonded to the end of the CSM specimens using 5-min epoxy. This specimen configuration was successful when the roller was positioned in the loose- and tight-constraint conditions. The SEA was highest in the tight-constraint condition. A tight-constraint to loose-constraint to no-constraint condition resulted in a lower SEA (see Tables I and II and Figs. 7 and 8).

Effect of crushing speed

No-constraint condition

The SEA was independent of changes in the crushing speed when the tests were conducted in the no-constraint condition (see Table III). For a comparison of the load-displacement traces recorded for a test conducted on a specimen in the no-constraint condition at loading rates of 0.5 and 5 cm/min, see Figures 9 and 10.

Loose-constraint condition

An increase in the crushing speed caused a decrease in the SEA, when the tests were conducted in the loose-constraint condition (see Table IV). For a comparison of the load-displacement traces recorded for a test conducted on a specimen in the loose-constraint condition at loading rates of 0.5 and 5 cm/min, see Figures 11 and 12.

Tight-constraint condition

An increase in the crushing speed caused a decrease in the SEA, when the tests were conducted in the tight-constraint condition (see Table V). For a comparison of the load-displacement traces recorded for a test conducted on a specimen in the tight-constraint condition at loading rates of 0.5 and 5 cm/min, see Figures 13 and 14.

Effect of profile radius

An increase in the profile radius caused a decrease in the SEA of the CSM material (see Table VI). For a comparison of the load-displacement traces recorded for a test conducted on a specimen using a profile block of radius of 0.635 cm and on a specimen using a profile block of radius 1.27 cm, see Figure 15.

The decrease in SEA with an increase in the profile radius is due to a specimen loaded in compression is crushed through the contact profile as defined by the profile block and it follows a smoother curve when the profile block has a radius of 1.27 cm as compared to a

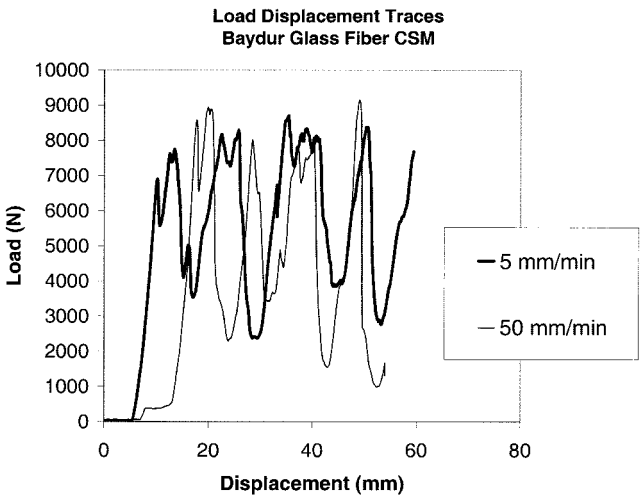

Figure 13 Load-displacement traces for a test conducted on CSM in the tight-constraint condition at loading rates of 0.5 and 5 cm/min.

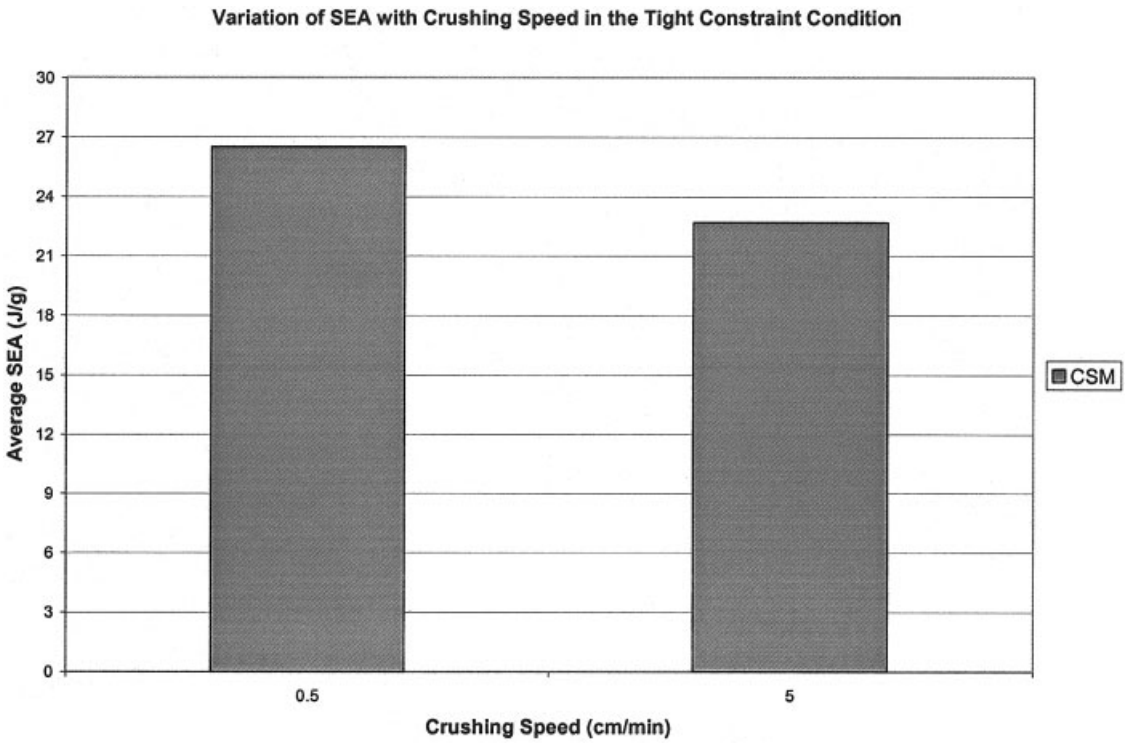

Figure 14 Variation of SEA with crushing speed for CSM in the tight-constraint condition.

TABLE VI
Experimental Data from Tests Conducted with a Profile Block of Radius 0.635 and 1.27 cm at 0.5-cm/min Loading Rate in the No-constraint Condition on CSM

Specimen no.	Specimen width (cm)	Profile radius (cm)	Constraint	Load rate (cm/min)	Initial peak load (N)	Maximum peak load (N)	Sustained crush load (N)	SEA (J/g)	Average SEA (J/g)
CSM-1	5.070	0.635	None	0.5	7478.2	9556.5	4829.1	10.79	
CSM-2	5.071	0.635	None	0.5	7867.3	9487.0	4657.5	10.25	
CSM-3	5.073	0.635	None	0.5	8157.8	9064.7	4443.9	9.71	
CSM-4	5.070	0.635	None	0.5	8334.2	9460.9	4560.6	10.10	
CSM-5	5.072	0.635	None	0.5	7986.5	9123.5	4615.4	10.15	10.20
CSM-31	5.093	1.27	None	0.5	3228.0	4182.3	2199.0	7.00	
CSM-32	5.109	1.27	None	0.5	3913.8	3913.8	1908.6	6.62	
CSM-33		1.27	None	0.5	3876.4	4179.0	2189.9	6.87	
CSM-34		1.27	None	0.5	3654.7	4000.0	2098.1	6.78	
CSM-35		1.27	None	0.5	3912.4	3999.8	2100.6	6.77	6.81

radius of 0.635 cm. Therefore, less energy is absorbed in bending it (see Fig. 16).

CONCLUSIONS

To identify and quantify the energy-absorbing mechanisms in candidate automotive composite materials, test methodologies were developed for conducting progressive crush tests on composite specimens that have simplified geometries. The test method development and experimental setup focused on isolating damage modes associated with frond formation that occurs in dynamic testing of composite tubes. Quasi-static progressive crush tests were conducted to quan-

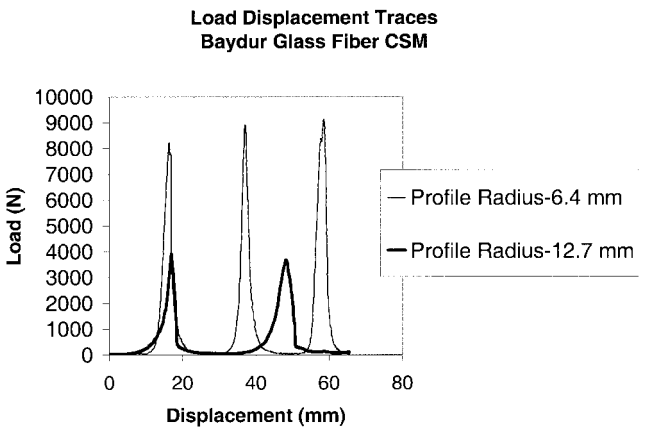

Figure 15 Load-displacement traces for a test conducted with a profile block of radius 0.635 and 1.27 cm on CSM.

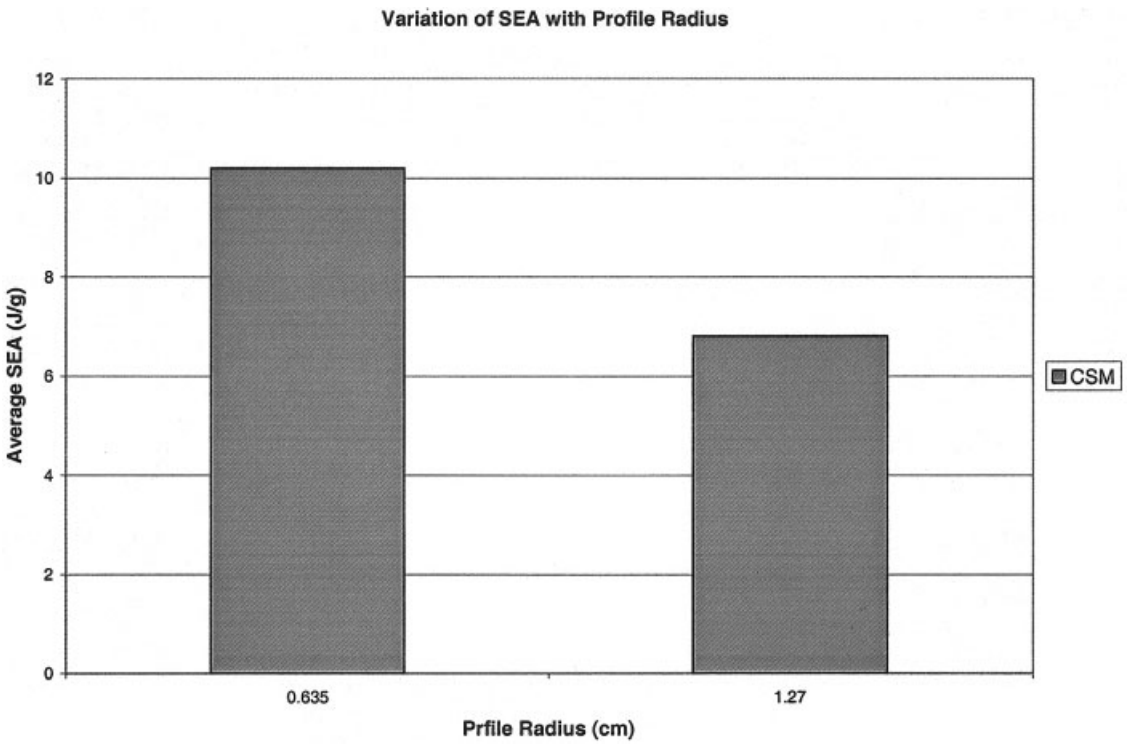

Figure 16 Variation of SEA with profile radius for SCM.

tify the effects of the profile radius, profile constraint, and loading rate on the SEA and failure modes of glass/polyurethane CSM composite plate specimens. An increase in the crushing speed caused a decrease in the SEA, when tested in the loose- and tight-constraint conditions. This confirmed the rate dependence of the SEA of CSM composites. An increase in the radius of the profile block caused a decrease in the SEA for the CSM specimens. The no-constraint condition resulted in the lowest SEA relative to the other constraint conditions.

Modifications to the basic specimen geometry were required when testing material systems having a low axial stiffness. For example, the tests conducted on the CSM material were only successful when the roller was positioned in the no-constraint condition. When the loose- or tight-constraint condition was attempted, the initial peak load increased and the CSM specimens buckled between the top plate and roller ways. The roller ways were unsuccessful in preventing out-of-plane buckling in the CSM material because of its low buckling strength. This resulted in having to use a metal push plate to reduce the unsupported specimen length. The metal plate was 76 mm in length and was bonded to the end of the CSM specimens using 5-min epoxy. This specimen configuration was successful when the roller was positioned in the loose- and tight-constraint conditions. The experimental data in conjunction with the test observations were used to develop analytical models for predicting the crashworthiness of automotive composite structures.

References

1. Hull, D. Sci Technol Rev Univ Wales 1988, 3, 23–30.
2. Thornton, P. H.; Edwards, P. J. J Comp Mater 1982, 16, 521–545.
3. Schmuesser, D. W.; Wickliffe, L. E. J Eng Mater Tech 1987, 109, 72–77.
4. Farley, G. L. In Proceedings of the 43rd American Helicopter Society Annual Forum, St. Louis, MO, 1987; pp 613–627.
5. Farley, G. L. J Comp Mater 1986, 20, 390–400.
6. Farley, G. L. J Comp Mater 1983, 17, 267–279.
7. Farley, G. L. J Comp Mater 1986, 20, 322–334.
8. Farley, G. L. In Proceedings of the ICCM 6; Matthews, F. L.; Buskell, N. C. R.; Hodgkinson, J. M.; Mortan, J., Eds.; Elsevier: London, UK, 1987; pp 3.57–3.66.
9. Hull, D. Comp Sci Tech 1991, 40, 377–421.
10. Hull, D. In Structural Crashworthiness; Jones, N.; Weirzbicki, T., Eds.; Butterworths: London, UK, 1983; pp 118–135.
11. Hamada, H.; Ramakrishna, S.; Maekawa, Z.; Nakamura, M. In Proceedings of the 10th Annual ASM/ESD Advanced Composite Conference, Dearborn, MI, Nov. 7–10, 1994; pp 511–522.
12. Hamada, H.; Ramakrishna, S. J Thermoplast Comp Mater 1996, 9, 259–279.
13. Farley, G. L.; Jones, R. M. J Comp Mater 1992, 26, 78–89.
14. Thornton, P. H. J Comp Mater 1979, 13, 247–262.
15. Ramakrishna, S.; Hamada, H.; Maekawa, Z.; Sato, H. J Therm Comp Mater 1995, 8, 323–344.
16. Farley, G. L. In 27th SDM Conference, 1986; submitted for publication to American Helicopter Society.
17. Ramakrishna, S.; Hull, D. Comp Sci Tech 1993, 49, 349–356.
18. Ramakrishna, S. Ph.D Thesis, University of Cambridge, UK, 1992.
19. Ramakrishna, S. J Reinf Plast Comp 1995, 14, 1121–1141.
20. Ramakrishna, S.; Hamada, H.; Hull, D In Impact and Dynamic Fracture of Polymers, ESIS19; Williams, J. G.; Pavan, A., Eds.; Mechanical Engineering: London, UK, 1995; pp 453–464.
21. Ramakrishna, S.; Hull, D. In Proceedings of the International Conference on Advances in Structural Testing, Analysis and

Design, Bangalore, India; Dattaguru, B., Ed.; Tata McGraw–Hill: New Delhi, India, 1990; pp 69–74.
22. Hamada, H.; Ramakrishn, S.; Maekawa, Z.; Nakamura, M.; Nishiwaki, T. In Proceedings of the 10th Annual ASM/ESD Advanced Composite Conference, Dearborn, MI, Nov. 7–10, 1994; pp 523–534.
23. Hamada, H.; Nakai, A.; Nakatani, T. In Proceedings of the First Canada–Japan Seminar on Composite Materials, Kyoto, Japan, 1996; pp 44.1–44.4.
24. Mamalis, A. G.; Yuan, Y. B.; Viegelahn, G. L. Int J Veh Des 1992, 13, 564–579.
25. Thornton, P. H.; Tao, W. H.; Robertson, R. E. In Advanced Composite Materials: New Development and Applications Conference Proceedings, Detroit, MI, Sept. 30–Oct. 3, 1991; pp 489–496.
26. Bannerman, D. C.; Kindervater, C. M. In Proceedings of the 4th International SAMPE European Chapter, Bordeaux, France, 1984; pp 155–167.
27. Thornton, P. H. J Comp Mater 1990, 24, 594–615.
28. Farley, G. L. J Comp Mater 1991, 25, 1314–1329.
29. Kindervater, C. M. In National Specialists Meeting, Composite Structures of the American Helicopter Society, Philadelphia, PA, March 23–25, 1983.
30. Lavoie, J. A.; Morton, J. NASA Contractor Report 4526, July 1993.
31. Starbuck, J. M.; Jacob, G. C.; Simunovic, S. Doc. No. 2000-01-1575; Future Car Congress: Crystal City, VA, 2000.